Int. J. Multiphase Flow Vol. 15, No. 1, pp. 97–118, 1989
Printed in Great Britain

0301-9322/89 $3.00 + 0.00
Pergamon Press/Elsevier

THEORY OF SURFACE DEPOSITION FROM A BINARY DILUTE VAPOR-CONTAINING STREAM, ALLOWING FOR EQUILIBRIUM CONDENSATION WITHIN THE LAMINAR BOUNDARY LAYER

J. L. CASTILLO† and D. E. ROSNER‡

High Temperature Chemical Reaction Engineering Laboratory, Department of Chemical Engineering, Yale University, New Haven, CT 06520, U.S.A.

(*Received* 7 *March* 1986; *in revised form* 5 *September* 1988)

Abstract—Deposition rates on solid targets cooled far below the dew point of undersaturated, dilute binary vapor and hot gas mainstreams have recently been found to be reduced and sharply surface temperature dependent compared to their pure vapor deposition counterparts. A rational yet tractable theory to account for such observations is formulated and exploited in particular cases of current practical interest; e.g. the deposition of trace multiple alkali sulfate vapors present in flowing combustion products. Our physicochemical model is based on the formation of a binary solution condensate aerosol near the deposition surface, with the resulting droplets collected by the mechanism of *thermophoresis*. The binary vapors, assumed here to be in local equilibrium with the solution aerosol phase, are collected by the familiar mechanism of Fick (concentration) diffusion across the prevailing laminar boundary layer (LBL) but we do not make the restrictive assumption that the Fick diffusivities are equal to the energy diffusivity of the carrier gas. As by-products of our calculation of the total (aerosol + vapor) deposition rate we obtain the BL position of condensation onset, as well as the structure of the LBL on either side of this binary "fog-locus". Illustrative predictions are shown for the effects of $Na_2SO_4(g)$ addition on salt deposition rates from combustion product streams containing a fixed amount of $K_2SO_4(g)$, on the assumption that the resulting $Na_2SO_4 + K_2SO_4$ droplets form nearly ideal solutions, having droplet thermophoretic diffusivities within two decades of the host gas momentum diffusivity, ν. With systematic corrections for the effects of (a) alkali salt vapor dissociation/equilibrium chemical reaction with the hydrocarbon combustion products and (b) slight solution non-ideality, the present theoretical formalism should be useful in accounting for binary nucleation onset effects observed in recent deposition rate experiments using alkali-seeded atmospheric pressure flat flames.

Key Words: vapor deposition, mass transport, boundary layer theory, multiphase flow, thermophoresis

1. INTRODUCTION—MOTIVATION

It is well-known that vapor mixtures capable of forming solution condensates will form aerosols under conditions such that either constituent vapor would itself be undersaturated. For this reason we expect that the deposition rate of multiple salts from flowing combustion gases will be influenced by the formation of solution condensate aerosols near the deposition surface when the surface is sufficiently far below the multiple salt dew point temperature. To anticipate such results and guide the design of experiments and presentation of the results of such experiments (currently underway in this laboratory; Liang *et al.* 1988) we have developed the theory outlined here, and illustrated it for air(-like) streams containing dilute amounts of $K_2SO_4(g) + Na_2SO_4(g)$. Deposition from multicomponent salt systems of this type is of considerable interest in a number of energy conversion and materials processing technologies. In particular, sea-salt ingested into aircraft, or marine, combustion turbines form such multisalt alkali sulfate vapor mixtures which, in turn, lead to corrosive condensate layers on the turbine blades (e.g. Rosner *et al.* 1979). Similarly, the products of *coal* combustion contain multiple condensible vapors capable of forming solution condensate aerosol droplets in the vicinity of, say, heat exchanger surfaces. These applications have motivated the extensions described here of our earlier deposition rate theories (Rosner *et al.* 1979; Castillo & Rosner 1988a). The first of these papers was confined to the limiting case [hereafter called "frozen

†On leave of absence from Department of Fundamental Physics, UNED, Aptdo 60141, Madrid 28080, Spain.
‡To whom all correspondence should be addressed.

boundary layer" (FBL)] of condensation only at the deposition surface itself. The second paper, which also considered equilibrium BL condensation but only for *unary* vapors, set the stage for the present extension.

1.1. Outline

In this paper we present a realistic but tractable theory of the deposition behavior of multicomponent dilute condensible vapor mixtures flowing near cold solid surfaces. We account for the possible condensation of these vapors within the thermal BL leading to the formation of multicomponent droplets which are then driven toward the cold surface by the local temperature gradient force (*thermophoresis*). The system is sketched in figure 1, the gas is undersaturated far from the cooled wall (1ϕ region) and the vapors condense within the thermal BL forming a condensated mist in local thermal equilibrium with the vapors (2ϕ region). The deposition rate on the wall is given by the diffusion flux of the vapors to the wall plus the deposition of condensate droplets driven by thermophoresis. The simplifying assumptions which underlie our theoretical model, and the associated equations are first developed in section 2. In section 3, we apply our mathematical model to a *binary* mixture of condensible vapors in steady laminar "wedge" flow of carrier gas, and the associated ordinary differential equations are obtained. In section 4, we then develop solutions to these equations; first for the degenerate case of no vapor condensation inside the BL (i.e. dispersed condensate *not* present) and then for the more interesting case in which local condensation occurs and equilibrium exists between the condensed droplets and the surrounding vapor. Representative results for binary mixtures of K_2SO_4 and Na_2SO_4 vapors dilute in high temperature air at atmospheric pressure are given in section 5. While illustrated here for the case of dilute binary vapors forming ideal solution droplets, the present deposition rate formulation is readily extended to multicomponent non-ideal systems of interest in many energy conversion—and materials processing—technologies.

2. MODEL FOR MULTICOMPONENT VAPORS

2.1. Underlying Assumptions and Validity Criteria

To obtain a tractable mathematical model for this apparently complex physical system the following simplifying assumptions will be adopted:

A.1. The amount of condensible vapor is very small with respect to the non-condensible (carrier) gas. Accordingly, the mixture velocity and temperature fields are not affected by the different processes (condensation, deposition) occurring in the relatively small amount of vapor.

A.2. The vapors behave as ideal gases at the low (partial) pressures considered.

A.3. The liquid mixtures (dispersed droplets or continuous liquid layers) formed by the different condensible components in the gas, behave as ideal solutions. Thus the partial molar volume of each component in solution is equal to its

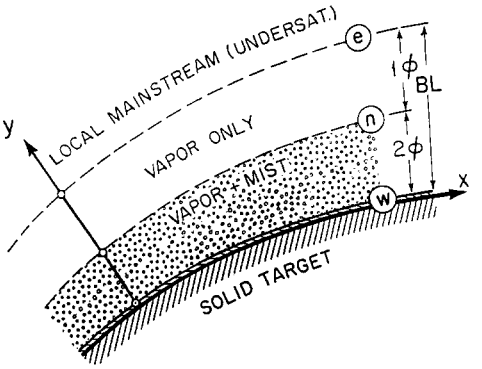

Figure 1. Schematic of the structure of the LBL near the deposition surface showing the inner zone of two-phase (aerosol condensate) flow; the primary *condensate* deposition mechanism is thermophoresis toward the cooled surface.

pure-component molar volume at the same temperature and pressure. This assumption is valid when the liquid components have similar molecular sizes and chemical character.

A.4. Whenever liquid and vapors co-exist, they are in local thermodynamical equilibrium (LTE); i.e. the residence time is much larger than the required time for such a two-phase system to reach LTE. By adopting this LTE approximation we free ourselves of the need to speculate about the kinetics of condensation or nucleation; i.e. we consider the local nucleation rate to be large compared to the dynamic process. For a discussion of this point, see appendix C and Castillo & Rosner (1988b). Furthermore, the equilibrium vapor pressure over a small liquid droplet will be taken to be the same as over a flat liquid layer with the same temperature and composition (i.e. the Kelvin effect will be neglected). In another paper (Castillo & Rosner 1988b) we have shown that, for alkaline-type vapors, the Kelvin effect is negligible for droplet radius $>0.1\ \mu$m. Accordingly, we need not be concerned with the size (or number density) of droplets in the two-phase region, but rather only with the total amount of condensible material in each phase (vapor and droplets).

A.5. We restrict ourselves to steady laminar flows and make the usual high Reynolds number BL approximations. Self-similarity will be assumed for the boundary conditions of interest here.

A.6. The thermodynamic properties of the gas (viscosity, thermal diffusivity etc.) will be considered approximately constant and equal to the values for the carrier gas evaluated at mainstream conditions. Also, the transport properties for vapor (Fick diffusion coefficients) and droplets (thermophoretic coefficient) will be taken to be constant. Finally, the total mixture density will be taken as a known constant, value, ρ_∞.†

A.7. Multicomponent and thermal (Soret) diffusion effects will be neglected for the *vapors*. Thus, the difference between the carrier gas and each vapor velocity is only due to the diffusion flux of the vapor down its own concentration gradient.

A.8. The droplets do not appreciably Brownian diffuse and the difference between the carrier gas and the droplet velocities is due only to a *thermophoretic drift* velocity, $\mathbf{v}_T$, of the droplets. $\mathbf{v}_T$ will be taken at each position as that corresponding to an isolated droplet in a uniform gas flow with the same temperature gradient.

A.9. The liquid deposit behaves as if it were motionless. Thus, the boundary condition (BC) for the gas at the macroscopic liquid surface will be taken to be the same as the BC on a corresponding rigid surface, and the deposit composition is governed by the *local* deposition fluxes. For very thin liquid layers (e.g. in the earliest stages of deposition) this approximation is expected to be adequate (cf. Rosner *et al.* 1983).

2.2. *Vapor/Liquid Equilibrium*

Wherever the vapors are in contact with the liquid phase we assume (A.4) they are in LTE. Here we develop the consequences of LTE when ideality can be assumed in both the vapor and liquid phases. For a more extensive treatment of this general topic, see, for example, Prausnitz *et al.* (1967) and Smith & Van Ness (1975).

†Gökoğlu & Rosner (1984) compared numerical results for heat and mass transfer in LBLs with an without property variations for vapors in air and proposed a simple correlation scheme. They showed that, in general, for the range $0.25 \leqslant T_w/T_e \leqslant 4$ and for Lewis numbers $(D/\alpha_h < 1)$ (as in our case), the results for mass transfer considering constant properties differ no more than 18% from the results using actual property variations. In particular, for K_2SO_4 vapors in air, the difference was $<10\%$ for the same range of temperature ratios. Thus, even for the lower values of T_w/T_e we have considered, the error we are making in the present analysis is acceptably small.

Under assumptions A.2 and A.3, we have

$$x_i = \frac{p_{v,i}}{p_{v,i}^{eq}}. \tag{1}$$

That is, at equilibrium, the mole fraction of component, i, in the solution, x_i, is equal to the ratio of the vapor pressure of i over the prevailing solution to the equilibrium vapor pressure of i over pure liquid† i at the same temperature.

Instead of working with partial vapor pressures it will be more convenient to deal with the vapor *mass fraction*, $\omega_{v,i} = \rho_{v,i}/\rho$, simply related to the vapor pressure for ideal gases through

$$\omega_{v,i} = \frac{1}{\rho} \cdot \left(\frac{p_{v,i} M_{v,i}}{RT} \right). \tag{2}$$

In the same way we can define an *equilibrium mass fraction*, $\omega_{v,i}^{eq}$, as the vapor mass fraction over a pure liquid i at the same temperature by

$$\omega_{v,i}^{eq} = \frac{1}{\rho} \cdot \left(\frac{p_{v,i}^{eq} M_{v,i}}{RT} \right) \tag{3}$$

which, once the density ρ is specified, is only a function of T. Then [1] can be written as

$$x_i = \frac{\omega_{v,i}}{\omega_{v,i}^{eq}}, \quad i = 1, \ldots N, \tag{4}$$

which is the equilibrium condition used in the following calculations.

Note that, due to the relation $\Sigma x_i = 1$, if we define

$$s \equiv \sum_{i=1}^{N} \frac{p_{v,i}}{p_{v,i}^{eq}} = \sum_{i=1}^{N} \frac{\omega_{v,i}}{\omega_{v,i}^{eq}} \tag{5}$$

then s is a measure of the degree of vapor phase saturation. When $s < 1$, the liquid cannot exist in equilibrium with the vapors. Thus, using assumption A.4, in general, we can divide the real space in two different regions (see figure 1): a single-phase region (no liquid droplets) in which $s < 1$; and a two-phase region (liquid droplets present) in equilibrium with the vapors, i.e. $s = 1$ everywhere and [4] is fulfilled for each component.

2.3. Droplet Thermophoresis

Thermophoresis is the phenomena of particle drift down a temperature gradient (analogous to the Soret effect in the diffusion of solute molecules through non-isothermal solutions). It is a rarified flow phenomena wherein small particles, suspended in a gas in which there exists a local temperature gradient, **grad** T, experience a force in the direction of $-$**grad** T (e.g. Fuchs 1964; Talbot 1981).

Thermophoretic transport can be described in terms of the difference, $\mathbf{v}_T$, between the particle and gas velocities, in an infinite gas with a uniform temperature gradient, once dynamical equilibrium is reached (i.e. when the local thermophoretic force is balanced by the local drag force). For particles whose radius is smaller than the mean-free-path of the gas molecues, $\mathbf{v}_T$ is normally written as

$$\mathbf{v}_T = \alpha_T D_{drop} \left[\frac{-\mathbf{grad} T}{T} \right] \tag{6}$$

but D_{drop} is formally included here only to emphasize the similarity between [6] and the ordinary diffusion velocity. Actually, the value of $\alpha_T D_{drop}$ does not really depend on D_{drop} (which, in fact, we have asymptotically taken as equal to zero, according to assumption A.8). Rather, it is droplet size independent and proportional to the gas momentum diffusivity ν_G; being $\approx 0.54\, \nu_G$ (Talbot 1981, [16], p. 476) in the limit we are considering.

†The pure liquid i at this temperature need not really exist. In such cases the concept of a hypothetical liquid should be used with the value of $p_{v,i}^{eq}$ computed by extrapolation from the real liquid region.

According to assumption A.8, we consider $\mathbf{v}_c = \mathbf{v}_G + \mathbf{v}_T$, with $\mathbf{v}_T$ given by [6], neglecting in this way particle inertia [i.e. considering the Stokes number for a particle to be very small; cf., for example, Fernandez de la Mora & Rosner (1982) and Rosner (1986)].

2.4. Conservation Equations for the Vapor and Condensate Mass Fractions

We consider a system in which there is an inert carrier gas (density ρ_{inert}), N condensible vapors (densities $\rho_{v,i}$, $i = 1, \ldots N$) and these same chemical substances in the condensate phase (densities $\rho_{c,i}$) in the form of liquid droplets. The governing conservation (balance) equations for these densities are

$$\frac{\partial \rho_{inert}}{\partial t} + \operatorname{div}\{\rho_{inert}\mathbf{v}_{inert}\} = 0, \tag{7}$$

$$\frac{\partial \rho_{v,i}}{\partial t} + \operatorname{div}\{\rho_{v,i}\mathbf{v}_{v,i}\} = -\dot{r}_i''' \tag{8}$$

and

$$\frac{\partial \rho_{v,i}}{\partial t} + \operatorname{div}\{\rho_{c,i}\mathbf{v}_c\} = \dot{r}_i''', \tag{9}$$

where $\dot{r}_i'''$ denotes the local (mass) condensation rate; i.e. the mass of vapor i being transformed into condensate i per unit time and volume.

Defining the total densities $\rho_G = \rho_{inert} + \Sigma\, \rho_{v,i}$ and $\rho = \rho_G + \Sigma\, \rho_{c,i}$ one finds

$$\frac{\partial \rho_G}{\partial t} + \operatorname{div}\{\rho_G\mathbf{v}_G\} = -\sum_{i=1}^{N} \dot{r}_i''' \tag{10}$$

and

$$\frac{\partial \rho}{\partial t} + \operatorname{div}\{\rho\mathbf{v}\} = 0. \tag{11}$$

Since the vapor mass fractions are defined with respect to the gas density, $\omega_{v,i} \equiv \rho_{v,i}/\rho_G$ will have to satisfy the following PDE:

$$\rho_G \frac{\partial \omega_{v,i}}{\partial t} + \rho_G\mathbf{v}_G \cdot \mathbf{grad}\, \omega_{v,i} = \operatorname{div}\{\rho_G D_{v,i}\, \mathbf{grad}\, \omega_{v,i}\} - \dot{r}_i''' + \omega_{v,i} \sum_{j=1}^{N} \dot{r}_j''', \tag{12}$$

where we have used assumption A.7; i.e. the difference beween $\mathbf{v}_{v,i}$ and $\mathbf{v}_G$ is the diffusion velocity of vapor i and therefore,

$$\rho_{v,i}(\mathbf{v}_{v,i} - \mathbf{v}_G) = \rho_{v,i}\mathbf{v}_{diff,i} = \mathbf{j}''_{diff,i} = -D_{v,i}\rho_G\, \mathbf{grad}\, \omega_{v,i}. \tag{13}$$

Similarly, since condensate mass fractions are defined with respect to the gas, $\omega_{c,i} \equiv \rho_{c,i}/\rho_G$ must satisfy the following PDE:

$$\rho_G \frac{\partial}{\partial t}\omega_{c,i} + \rho_G(\mathbf{v}_G + \mathbf{v}_T) \cdot \mathbf{grad}\, \omega_{c,i} = -\omega_{c,i} \operatorname{div}\{\rho_G\mathbf{v}_T\} + \dot{r}_i''' + \omega_{c,i} \sum_{j=1}^{N} \dot{r}_j''', \tag{14}$$

where we have used assumption A.8; i.e. the condensate velocity $\mathbf{v}_c$ differs from the gas velocity by the thermophoretic velocity $\mathbf{v}_T$,

$$\mathbf{v}_c = \mathbf{v}_G + \mathbf{v}_T. \tag{15}$$

For very dilute systems ($\omega_{v,i} \ll 1$, $\omega_{c,i} \ll 1$) (cf. assumption A.1) we can take $\rho_{inert} \approx \rho_G \approx \rho$, $\mathbf{v}_{inert} \approx \mathbf{v}_G \approx \mathbf{v}$. Considering the gas to be incompressible and invoking constant diffusion coefficients (assumption A.6), PDEs [12] and [14] reduce to

$$\frac{\partial \omega_{v,i}}{\partial t} + \mathbf{v} \cdot \mathbf{grad}\, \omega_{v,i} = D_{v,i} \operatorname{div}\{\mathbf{grad}\, \omega_{v,i}\} - \frac{\dot{r}_i'''}{\rho} \tag{16}$$

and

$$\frac{\partial \omega_{c,i}}{\partial t} + (\mathbf{v} + \mathbf{v}_T) \cdot \mathbf{grad}\, \omega_{c,i} = -\omega_{c,i} \operatorname{div} \mathbf{v}_T + \frac{\dot{r}_i'''}{\rho}, \tag{17}$$

where we have neglected the third r.h.s. terms in [12] and [14] with respect to the second r.h.s. terms due to the fact that $\omega_{v,i} \ll 1$ and $\omega_{c,i} \ll 1$. Equations [16] and [17], together with the equilibrium conditions [4] (which allow us to compute $\dot{r}_i'''$), determine the composition of the system.

On the other hand, [11] reduces to the usual local incompressibility condition

$$\operatorname{div} \mathbf{v} = 0. \tag{18}$$

2.5. *Conditions Across the "Interface" Between Single-phase and Two-phase Regions*

Across the "surface" separating the two spatial regions mentioned in the title, the mass flux of each component must be continuous. Thus, if $\mathbf{n}$ denotes the unit vector normal to this hypothetical surface (pointing, say, towards the single-phase region) this condition can be expressed as

$$\mathbf{n} \cdot (\rho_{v,i}\mathbf{v}_{v,i} + \rho_{c,i}\mathbf{v}_{c,i})^{2\phi} = (\rho_{v,i}\mathbf{v}_{v,i})^{1\phi} \cdot \mathbf{n}, \quad i = 1, \ldots, N. \tag{19}$$

Since, in a steady state, it can be shown that $\rho_{c,i}$ is equal to zero at this surface (only when $\mathbf{v}_c \cdot \mathbf{n} = 0$, $\rho_{c,i}^{2\phi}$ could be different from zero, but this is not our case), it follows from [13] that

$$\mathbf{n} \cdot (\rho_{v,i}\mathbf{v} - D_{v,i}\rho \, \mathbf{grad} \, \omega_{v,i})^{2\phi} = \mathbf{n} \cdot (\rho_{v,i}\mathbf{v} - D_{v,i}\rho \, \mathbf{grad} \, \omega_{v,i})^{1\phi}. \tag{20}$$

However, under assumption A.1, ρ and $\mathbf{v}$ are continuous, and so is $\rho_{v,i}$ (otherwise $\mathbf{v}_{diff,i}$ would be infinite), thus we obtain:

$$(\mathbf{n} \cdot \mathbf{grad} \, \omega_{v,i})^{2\phi} = (\mathbf{n} \cdot \mathbf{grad} \, \omega_{v,i})^{1\phi}, \quad i = 1, \ldots, N. \tag{21}$$

Relation [21] for each component allows us to connect the solutions in the two-phase (2ϕ) region with the solution in the adjacent single-phase (1ϕ) region. Note that $\mathbf{n} \cdot \mathbf{grad} \, \omega_{c,i}$ and $\mathbf{n} \cdot \mathbf{grad}(\mathbf{n} \cdot \mathbf{grad} \, \omega_{v,i})$ are discontinuous across the $1\phi/2\phi$ interface due to the discontinuity of $\dot{r}_i'''$.

2.6. *Vapor and Particle Fluxes at the Wall*

When a cooler solid surface, held at a constant temperature, T_w, is introduced into the gas flow, momentum and thermal BLs are generated accommodating the system to the BCs at the wall. Also, a diffusion BL will appear around the body and vapors will deposit on its surface if its temperature is below the dew point temperature. Under these circumstances, if $\mathbf{n}_w$ denotes the unit vector normal to the wall pointing into the gas phase, the flux of vapor i to this wall will be

$$j''_{v,i;w} = -\rho_{v,i}\mathbf{v}_{v,i} \cdot \mathbf{n}_w. \tag{22}$$

On the other hand, if the surface temperature is sufficiently low a two-phase region will appear adjacent to the body and its droplets will deposit in such a way that

$$j''_{c,i;w} = -\rho_{c,i}\mathbf{v}_{c,i} \cdot \mathbf{n}_w. \tag{23}$$

Taking into account the dynamic BC at the solid wall ($\mathbf{n}_w \cdot \mathbf{v} = 0$), together with [13] and [15], these fluxes become

$$j''_{v,i;w} = D_{v,i}\rho \, \mathbf{n}_w \cdot (\mathbf{grad} \, \omega_{v,i})_w \tag{24}$$

and

$$j''_{c,i;w} = -\rho\omega_{c,i;w}\mathbf{v}_{T,w} \cdot \mathbf{n}_w. \tag{25}$$

Under assumption A.4 the liquid deposit is at equilibrium with the vapors, so from [4]:

$$\frac{\omega_{v,i;w}}{\omega_{v,i}^{eq}(T_w)} = x_{i,dep}. \tag{26}$$

Using assumption A.9, the deposit composition is governed by the deposition fluxes, i.e.

$$x_{i,dep} = \frac{j''_{v,i;w} + j''_{c,i;w}}{M_{v,i}} \cdot \left(\sum_{j=1}^{N} \frac{j''_{v,j;w} + j''_{c,j;w}}{M_{v,j}} \right)^{-1}. \tag{27}$$

The droplets arriving at the wall are also in equilibrium with the prevailing vapors. Then

$$x_{i,\text{drop};w} \equiv \frac{\omega_{c,i;w}}{M_{v,i}} \cdot \left(\sum_{j=1}^{N} \frac{\omega_{c,j;w}}{M_{v,j}} \right)^{-1} = \frac{\omega_{v,i;w}}{\omega_{v,i}^{eq}(T_w)}, \quad [28]$$

i.e. the droplets at the wall have the same composition as the macroscopic liquid deposit. Using this relation in [25] and [27] we obtain

$$\frac{\omega_{v,i;w}}{\omega_{v,i}^{eq}(T_w)} = \frac{j''_{v,i;w}}{M_{v,i}} \cdot \left(\sum_{j=1}^{N} \frac{j_{v,j;w}}{M_{v,j}} \right)^{-1}, \quad i = 1, \ldots, N, \quad [29]$$

with $j''_{v,i;w}$ given by [24].

Equation [29] together with [24] and [25] are not only useful as BCs at the wall, they also determine the deposition fluxes onto the wall. Note that all the variables could depend on the position along the deposition surface.

2.7. Minimum Wall Temperature for Nucleation Onset

According to assumption A.4, the deposit, if it exists (i.e. if the wall temperature is lower than the corresponding dew point temperature) is at equilibrium with the vapors, therefore $s = 1$ at the wall. If the wall temperature is not too low, the wall is the only position at which liquid could exist; i.e. $s = 1$ only at the wall and $s < 1$ everywhere else ($\mathbf{n}_w \cdot \mathbf{grad}\, s < 0$). In this case, there are no droplets in the BL at all ($\omega_{c,i} = 0$ and $\dot{\omega}_i''' = 0$, everywhere) and the deposition is due only to vapor diffusion, and is given by [24].

On the other hand, if the wall temperature is sufficiently low, a two-phase region appears adjacent to the body. In this region, droplets and vapors co-exist at equilibrium; i.e. $s = 1$ everywhere inside this two-phase region ($\mathbf{n}_w \cdot \mathbf{grad}\, s = 0$). Droplets also deposit on the surface and the total deposition rate is given by [24] and [25]. Therefore, it is clear that the boundary between both two types of behavior corresponds to the case in which there are no droplets within the BL but

$$\mathbf{n}_w \cdot (\mathbf{grad}\, s)_w = 0, \quad [30]$$

with the deposition rate still given by [24]. That is, the "interface" between the single-phase and the two-phase regions lies just at the wall. With a further decrease in T_w this "interface" detaches from the wall and moves away from it, expanding the two-phase region as T_w decreases. The same phenomenon (growth in extent of the two-phase region) can be achieved at constant wall temperature by increasing the amount of condensible vapors in the mainstream.

3. SELF-SIMILAR FORM OF BALANCE EQUATIONS FOR BINARY VAPORS IN LAMINAR WEDGE FLOWS

3.1. Host (Carrier Gas) Flow-field

The potential flow (external solutions) which corresponds to the inviscid, incompressible fluid flow past a wedge (figure 2) with included angle $\pi\beta$ is given by

$$u_e(x) = ax^m, \quad [31]$$

where a is a constant and $\beta = 2m/(m+1)$. Two-dimensional stagnation flow, as well as the laminar BL on a flat plate at zero incidence, constitute particular cases of wedge flow—the former for $\beta = 1$ (i.e. $m = 1$) and the latter for $\beta = 0$ (i.e. $m = 0$). Moreover, the case $\beta = 1/2 (m = 1/3)$ can easily be transformed into the rotationally symmetrical stagnation point flow (Schlichting 1968, p. 150) if we put $\eta(\text{wedge}) = \eta(\text{rot. symm.}) \sqrt{2}$.

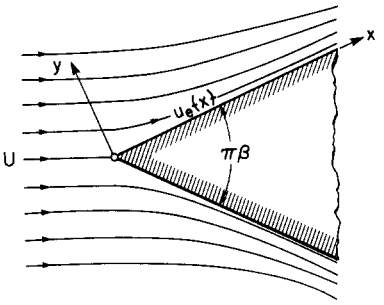

Figure 2. Steady incompressible viscous fluid flow past a cooled, solid wedge of opening angle $\pi\beta$; $Re_x^{1/2} \gg 1$.

As in any two-dimensional motion, the BL equations are given by

$$u\frac{\partial u}{\partial x} + v\frac{\partial u}{\partial y} = u_e\frac{du_e}{dx} + \nu\frac{\partial^2 u}{\partial y^2} \qquad [32]$$

and

$$\frac{\partial u}{\partial x} + \frac{\partial v}{\partial y} = 0 \qquad [33]$$

and BCs: $u = v = 0$ at $y = 0$ and $u = u_e(x)$ at $y = \infty$. The similarity variable η which leads to the ODEs is

$$\eta \equiv \frac{y}{x}\cdot\left(\frac{u_e(x)x}{\nu}\right)^{1/2} = y\left(\frac{ax^{m-1}}{\nu}\right)^{1/2}. \qquad [34]$$

The equation of local mass conservation, [33], is satisfied automatically by introducing a stream function, given by

$$\psi(x, y) = (\nu a)^{1/2}x^{(m+1)/2}\cdot f(\eta). \qquad [35]$$

Thus, the fluid velocity components become

$$u = \frac{\partial\psi}{\partial y} = ax^m f'(\eta) = u_e f'(\eta) \qquad [36]$$

and

$$v = \frac{-\partial\psi}{\partial x} = -\frac{m+1}{2}\cdot(\nu a x^{m-1})\cdot\left(f + \frac{m-1}{m+1}\eta f'\right), \qquad [37]$$

where primes denote differentiation with respect to η. Introducing these values into the x-momentum equation [32] and dividing by $a^2x^{(2m-1)}$, we obtain the following well-known (Blasius, Falkner-Skan) ODE for $f(\eta)$:

$$f''' + \frac{m+1}{2}\cdot ff'' + m[1 - (f')^2] = 0 \qquad [38]$$

with BCs:

$$@\ \eta = 0,\quad f = f' = 0 \qquad [39]$$

and

$$@\ \eta = \infty,\quad f' = 1. \qquad [40]$$

3.2. Temperature Field

In a steady state, using BL approximations (assumption A.5), and assumptions A.1† and A.6, the PDE which governs the fluid mixture temperature distribution is

$$u\frac{\partial T}{\partial x}+v\frac{\partial T}{\partial y}=\alpha_h\cdot\frac{\partial^2 T}{\partial y^2}, \tag{41}$$

α_h being the thermal diffusivity.

We seek a "similar" solution of the form $T\{x, y\}=T\{\eta\}$; thus, when the wall temperature is held constant and equal to T_w, we postulate

$$T=T_w+(T_\infty-T_w)\cdot\theta\{\eta\}, \tag{42}$$

with T_∞ being the temperature at the mainstream, far from the wall. Accordingly, the BC on θ can be expressed as

$$\theta\{0\}=0 \quad \text{and} \quad \theta\{\infty\}=1. \tag{43}$$

Using [34], [36], [37] and [42] in [41] we find that $\theta\{\eta\}$ must satisfy the following well-known (Polhausen) ODE:

$$\theta''+\frac{m+1}{2}\cdot \mathrm{Pr} f\theta'=0, \tag{44}$$

where Pr is the Prandtl number (ν/α_h) of the gas mixture. The solution of [44] with BCs [43] may be written (e.g. Spalding & Evans 1961) as

$$\theta\{\eta\}=\frac{1}{\delta_T}\cdot\int_0^\eta \exp\left[-\frac{m+1}{2}\cdot\mathrm{Pr}\cdot\int_0^\varphi f\{\xi\}\,d\xi\right]d\varphi \tag{45}$$

with

$$\delta_T\equiv\int_0^\infty \exp\left[-\frac{m+1}{2}\cdot\mathrm{Pr}\cdot\int_0^\varphi f\{\xi\}\,d\xi\right]d\varphi. \tag{46}$$

For a description of the computation of δ_T see the end of section 4.1.

3.3. Mass Fraction Equations and the Prediction of Deposition Rate

Assuming $\omega_{v,i}=\omega_{v,i}\{\eta\}$ and using [34], [36] and [37] in [16], together with the BL approximation (A.5), we find that each vapor mass fraction must satisfy the second-order ODE

$$\frac{d^2\omega_{v,i}}{d\eta^2}+\frac{m+1}{2}\mathrm{Sc}_i f\cdot\frac{d\omega_{v,i}}{d\eta}=\mathrm{Sc}_i\cdot\dot\omega_i''', \tag{47}$$

where $\mathrm{Sc}_i\equiv\nu/D_{v,i}$ is the Schmidt number for vapor i and

$$\dot\omega_i'''\{\eta\}\equiv\frac{\dot r_i'''\{x, y\}}{\rho u_e\{x\}}\cdot x=\frac{\dot r_i'''\{x, y\}}{\rho a x^{m-1}}. \tag{48}$$

Using the same relation in [17] and taking into account [6] we find that the *condensate* mass fraction must satisfy the first-order ODE

$$A\frac{d\omega_{c,i}}{d\eta}+B\omega_{c,i}=-\dot\omega_i''', \tag{49}$$

†It is easily shown that the effect of the latent heat of phase change can be neglected when $(\omega_{v,\infty}-\omega_{v,w})\ll(\alpha_h/D_v)^{1/3}\{[M_v c_p(T_\infty-T_w)]/\Lambda\}$. In our calculations the r.h.s. is of the order of unity, whereas the l.h.s. $\approx 10^{-3}$. Therefore, the required inequality holds.

where

$$A(\eta) \equiv \frac{m+1}{2} \cdot f + \frac{\alpha}{T} \cdot \frac{dT}{d\eta} \tag{50}$$

and

$$B(\eta) \equiv \frac{\alpha}{T}\left[\frac{d^2T}{d\eta^2} - \frac{1}{T}\left(\frac{dT}{d\eta}\right)^2\right], \tag{51}$$

$$\alpha \equiv \frac{\alpha_T D_{drop}}{v} \tag{52}$$

In the two-phase region, the equilibrium conditions [4] for a binary system transform to

$$\frac{\omega_{v,1}}{\omega_{v,1}^{eq}} = \frac{\omega_{c,1}}{\omega_{c,1} + r_m \omega_{c,2}} \tag{53}$$

and

$$\frac{\omega_{v,1}}{\omega_{v,1}^{eq}} + \frac{\omega_{v,2}}{\omega_{v,2}^{eq}} = 1, \tag{54}$$

where r_m is the molecular weight ratio $M_{v,1}/M_{v,2}$. Equations [47] and [49] together with [53] and [54] determine the vapor and condensate distributions of the two species, as well as the values of $\dot{\omega}_i'''$ $(i = 1, 2)$.

Using [34] in [24] the local mass deposition rate of vapor i at the wall ($x = 0$, i.e. $\eta = 0$) will be

$$j''_{v,i;w}(x) = \frac{\rho}{Sc_i} \cdot (avx^{m-1})^{1/2}\left(\frac{d\omega_{v,i}}{d\eta}\right)\bigg|_{\eta=0}. \tag{55}$$

Note that although the deposition rate depends on x under the present conditions the composition of the depositing vapors is the same over the entire surface. The *ratio* $j''_{v,1;w}/j''_{v,2;w}$ does not depend on x. If there are also droplets, the mass deposition of component i in droplet form, from [25], taking into account [6], [42] and [45], will be

$$j''_{c,i;w}(x) = \rho\alpha \cdot \frac{T_\infty - T_w}{T_w \delta_T} \cdot (avx^{m-1})^{1/2} \omega_{c,i}(\eta = 0). \tag{56}$$

We can define a convenient non-dimensional average deposition rate over a length L measured along x from the stagnation point, by

$$\mathscr{J}_{v,i} = \frac{m+1}{2\rho}(avL^{m+1})^{-1/2} \cdot \int_0^L j''_{v,i;w}(x)\, dx \tag{57}$$

and a similar expression for $\mathscr{J}_{c,i}$. Under the present conditions,

$$\mathscr{J}_{v,i} = \frac{1}{Sc_i} \cdot \frac{d\omega_{v,i}}{d\eta}\bigg|_{\eta=0} \tag{58}$$

and

$$\mathscr{J}_{c,i} = \frac{T_\infty - T_w}{T_w \delta_T} \cdot \alpha \omega_{c,i}(\eta = 0). \tag{59}$$

Furthermore, the equilibrium between the liquid deposit and the vapor, [29] can be written in the form

$$\frac{\omega_{v,1;w}}{\omega_{v,1}^{eq}(T_w)} = \frac{\mathscr{J}_{v,1}}{\mathscr{J}_{v,1} + r_m \mathscr{J}_{v,2}} \tag{60}$$

and

$$\frac{\omega_{v,1;w}}{\omega_{v,1}^{eq}(T_w)} + \frac{\omega_{v,2;w}}{\omega_{v,2}^{eq}(T_w)} = 1. \tag{61}$$

The total non-dimensional mass deposition rate (droplet form + vapor flux) of substance i will be

$$\mathscr{J}_i = \mathscr{J}_{v,i} + \mathscr{J}_{c,i}. \qquad [62]$$

Note that [61] is only necessary when there are no droplets ($\omega_{c,i} = 0$); i.e. the two-phase region does not exist. Otherwise, this condition is a particular case of [54] applied at the wall.

4. ANALYTICAL AND NUMERICAL METHODS

4.1. "Frozen" Boundary Layer (FBL)

When there is no droplet formation within the BL, $\dot{\omega}_i''' = 0$ and $\omega_{c,i} = 0$, the solution of [47] can be written in the form

$$\omega_{v,i} = \omega_{v,i;w} + (\omega_{v,i;\infty} - \omega_{v,i;w}) \cdot \Gamma_i(\eta, 0), \quad i = 1, 2, \qquad [63]$$

where

$$\Gamma_i(\eta,\phi) = \frac{1}{\delta_i(\phi)} \cdot \int_\phi^\eta \exp\left[-\frac{m+1}{2} \cdot \mathrm{Sc}_i \cdot \int_\phi^\varphi f(\xi)\, d\xi \right] d\varphi \qquad [64]$$

and

$$\delta_i(\phi) = \int_\phi^\infty \exp\left[-\frac{m+1}{2} \cdot \mathrm{Sc}_i \cdot \int_\phi^\varphi f(\xi)\, d\xi \right] d\varphi. \qquad [65]$$

Therefore, the non-dimensional deposition rate of vapor i, given by [58], becomes

$$\mathscr{J}_{v,i} = \frac{\omega_{v,i;\infty} - \omega_{v,i;w}}{\mathrm{Sc}_i \cdot \delta_i(0)}. \qquad [66]$$

These two equations (for $i = 1$ and 2), together with the equilibrium conditions [60] and [61], form an algebraic system of four equations with four unknowns ($\mathscr{J}_{v,i}$, $\omega_{v,i;w}$) which can be solved once $\omega_{v,i;\infty}$, $\omega_{v,i}^{eq}(T_w)$, Sc_i, r_m and $\delta_i(0)$ are known.

From [36], $f' = u/u_e$ and $f' \to 1$ when $\eta \to \infty$. In practice, f' reaches a value sufficiently near unity for a finite value of η. Thus, suppose, in general,

$$f = \eta - b \quad \text{for } \eta \geqslant \eta_\infty, \qquad [67]$$

b being a constant. Then from its definition, [65] we obtain

$$\begin{aligned} \delta_i(0) = {} & \int_0^{\eta_\infty} \exp\left[-\frac{m+1}{2} \cdot \mathrm{Sc}_i \int_0^\varphi f(\xi)\, d\xi \right] \cdot d\varphi \\ & + \exp\left[\frac{m+1}{4} \mathrm{Sc}_i (\eta_\infty - b) \right] \exp\left[-\frac{m+1}{2} \cdot \mathrm{Sc}_i \cdot \int_0^{\eta_\infty} f(\xi)\, d\xi \right] \\ & \times \left\{ \left[\frac{\pi}{(m+1)} \cdot \frac{1}{\mathrm{Sc}_i} \right]^{1/2} - \int_0^{\eta_\infty - b} \exp\left[-\frac{m+1}{4} \mathrm{Sc}_i \cdot \xi^2 \right] d\xi \right\}. \end{aligned} \qquad [68]$$

This equation is also valid for δ_T just changing Sc_i to Pr; see [46].

We have computed the value of $\delta_i(0)$ and δ_T using Simpson's algorithm. The necessary values of $f(\eta)$ were obtained using Taylor's expansion, employing the values of f, f', f'' and f''' at given η-values. The quantities f, f' and f'' are tabulated (e.g. Schlichting 1968, table 7.1, p. 129) for $m = 0$ (in this case, $\eta_\infty = 7.8$; $b = 1.72077$) and (Schlichting 1968, table 5.1, p. 90) for $m = 0$ ($\eta_\infty = 3.8$; $b = 0.6482$) and $m = 1/3$ ($\eta_\infty = 5.6$; $b = 0.9855$), in this last case taking into account the different non-dimensionalization, η (here) $= \sqrt{3}\zeta$ (Schlichting) and f (here) $= \sqrt{3}\phi$ (Schlichting) and the value of f'' obtained from [38]. Moreover, values of [68] for some specified values of m and Sc_i can be found in Evans (1961, table 3, p. 33). It should be noted that due to the different similarity variable used, $\delta_i(0) = [2/m + 1]^{1/2} \times$ (Evans' tabulated value)$^{-1}$, and $\beta = 2m/(m+1)$. We have used Evans' table to check our computer program, obtaining perfect agreement for the values of the Euler parameter m (0, 1 and 1/3) of principal interest here.

4.2. Condensation Within the Boundary Layer

Let us assume a two-phase region exists adjacent to the wall in which there are droplets at local equilibrium with the vapors extending into the BL until a position given by $\eta = \eta_n$, i.e. the "interface" between the single-phase and the two-phase region is located at η_n. Then, for $\eta \geqslant \eta_n$, the solution of [47] with $\dot{\omega}_i''' = 0$, is

$$\omega_{v,i} = \omega_{v,i;n} + (\omega_{v,i;\infty} - \omega_{v,i;n}) \cdot \Gamma_i(\eta, \eta_n) \quad \begin{cases} i = 1, 2 \\ \eta \geqslant \eta_n \end{cases} \tag{69}$$

with $\Gamma_i(\eta, \eta_n)$ given by [64] and $\omega_{v,i;n} \equiv \omega_{v,i}(\eta_n)$.

For $\eta \leqslant \eta_n$, although the solution could be expressed in the form of quadratures (see appendix B), it is better to transform the system given by [47], [49], [53] and [54] to a system of ODEs for $x_1 = \omega_{v,1}/\omega_{v,1}^{eq}$ and $\omega_{c,1}$. After some manipulations, we obtain

$$\left[\omega_{v,2}^{eq} + \left(\frac{1}{x_1} - 1\right) \cdot \frac{Sc_2 \omega_{v,1}^{eq}}{Sc_1 r_m}\right] \cdot \frac{d^2 x_1}{d\eta^2} + \left[\left(\frac{1}{x_1} - 1\right) \frac{Sc_2}{r_m Sc_1} \cdot \left(2 \frac{d\omega_{v,1}^{eq}}{d\eta} + \frac{m+1}{2} Sc_1 f \omega_{v,1}^{eq}\right)\right.$$

$$\left. + 2 \frac{d\omega_{v,2}^{eq}}{d\eta} + \frac{m+1}{2} Sc_2 f \omega_{v,2}^{eq} + A \frac{\omega_{c,1} Sc_2}{x_1^2 r_m}\right] \frac{dx_1}{d\eta}$$

$$+ (1 - x_1)\left[\frac{Sc_2}{r_m Sc_1} \cdot \left(\frac{d^2 \omega_{v,1}^{eq}}{d\eta^2} + \frac{m+1}{2} Sc_1 f \frac{d\omega_{v,1}^{eq}}{d\eta}\right) - \frac{d^2 \omega_{v,2}^{eq}}{d\eta^2} - \frac{m+1}{2} \cdot Sc_2 f \cdot \frac{d\omega_{v,2}^{eq}}{d\eta}\right] = 0 \tag{70}$$

and

$$\left[\frac{Sc_2}{r_m \omega_{v,2}^{eq}}\left(\frac{1}{x_1} - 1\right) + \frac{Sc_1}{\omega_{v,1}^{eq}}\right] \cdot A \cdot \frac{d\omega_{c,1}}{d\eta} + \left\{\left[\frac{Sc_2}{r_m \omega_{v,2}^{eq}}\left(\frac{1}{x_1} - 1\right) + \frac{Sc_1}{\omega_{v,1}^{eq}}\right] B - A \cdot \frac{Sc_2}{x_1^2 r_m \omega_{v,2}^{eq}} \cdot \frac{dx_1}{d\eta}\right\} \omega_{c,1}$$

$$+ \frac{dx_1}{d\eta} \cdot \left[\frac{2}{\omega_{v,1}^{eq}} \frac{d\omega_{v,1}^{eq}}{d\eta} - \frac{2}{\omega_{v,2}^{eq}} \frac{d\omega_{v,2}^{eq}}{d\eta} + \frac{m+1}{2} f(Sc_1 - Sc_2)\right]$$

$$+ \frac{x_1}{\omega_{v,1}^{eq}} \cdot \left[\frac{d^2 \omega_{v,1}^{eq}}{d\eta^2} + \frac{m+1}{2} \cdot Sc_1 \cdot f(\eta) \frac{d\omega_{v,1}^{eq}}{d\eta}\right] + \frac{1 - x_1}{\omega_{v,2}^{eq}} \cdot \left[\frac{d^2 \omega_{v,2}^{eq}}{d\eta^2} + \frac{m+1}{2} \cdot Sc_2 \cdot f(\eta) \frac{d\omega_{v,2}^{eq}}{d\eta}\right] = 0 \tag{71}$$

with $\omega_{v,i}^{eq}$ being a function of η through its temperature dependence; i.e.

$$\omega_{v,i}^{eq} = \frac{1}{\rho} \cdot \frac{p_{v,i}^{eq}(T) M_{v,i}}{RT} \tag{72}$$

and the functions $A(\eta)$ and $B(\eta)$ are given by [50] and [51], respectively.

On the other hand, the continuity of mass flux of each component across the "interface", [21] becomes

$$\left.\frac{d\omega_{v,i}}{d\eta}\right|_{\eta_n}^{1\phi} = \left.\frac{d\omega_{v,i}}{d\eta}\right|_{\eta n}^{2\phi}. \tag{73}$$

Using [69] for computing the value at the single-phase region, we get, at $\eta = \eta_n$:

$$x_1 = \left[\frac{\omega_{v,1;\infty}}{\omega_{v,1}^{eq} \delta_1(\eta_n)} + \frac{\omega_{v,2;\infty} - \omega_{v,2}^{eq}}{\omega_{v,2}^{eq} \delta_2(\eta_n)} - \frac{1}{\omega_{v,2}^{eq}} \frac{d\omega_{v,2}^{eq}}{d\eta}\right] \cdot \left[\frac{1}{\omega_{v,1}^{eq}} \frac{d\omega_{v,1}^{eq}}{d\eta} - \frac{1}{\omega_{v,2}^{eq}} \frac{d\omega_{v,2}^{eq}}{d\eta} + \frac{1}{\delta_1(\eta_n)} - \frac{1}{\delta_2(\eta_n)}\right]^{-1} \tag{74}$$

and

$$\frac{dx_1}{d\eta} = \frac{\omega_{v,1;\infty} - \omega_{v,1}^{eq} x_1}{\omega_{v,1}^{eq} \delta_1(\eta_n)} - \frac{x_1}{\omega_{v,1}^{eq}} \cdot \frac{d\omega_{v,1}^{eq}}{d\eta} \quad @\ \eta = \eta_n. \tag{75}$$

Also, from their definitions,

$$\omega_{v,1;n} = x_1 \omega_{v,1}^{eq} \quad @\ \eta = \eta_n \tag{76}$$

and

$$\omega_{v,2;n} = (1 - x_1)\omega_{v,2}^{eq} \quad @\ \eta = \eta_n, \tag{77}$$

and, as stated earlier,

$$\omega_{c,1}(\eta_n) = 0. \tag{78}$$

The deposition rates of vapors and droplets, [58] and [59], become

$$\mathcal{J}_{v,1} = \frac{1}{Sc_1} \cdot \left[\omega_{v,1}^{eq} \frac{dx_1}{d\eta} + x_1 \frac{d\omega_{v,1}^{eq}}{d\eta} \right]_{\eta=0}, \tag{79}$$

$$\mathcal{J}_{v,2} = \frac{1}{Sc_2} \cdot \left[(1 - x_1) \frac{d\omega_{v,2}^{eq}}{d\eta} - \omega_{v,2}^{eq} \frac{dx_1}{d\eta} \right]_{\eta=0}, \tag{80}$$

$$\mathcal{J}_{c,1} = \frac{T_\infty - T_w}{T_w \delta_T} \cdot \alpha \omega_{c,1}(\eta = 0) \tag{81}$$

and

$$\mathcal{J}_{c,2} = \frac{T_\infty - T_w}{T_w \delta_T} \cdot \alpha \cdot \left[\frac{1 - x_1}{x_1 r_m} \cdot \omega_{c,1} \right]_{\eta=0}. \tag{82}$$

The total deposition rate is given by

$$\mathcal{J}_i = \mathcal{J}_{v,i} + \mathcal{J}_{c,i}. \tag{83}$$

Finally, the equilibrium between the liquid deposit and the vapors, [60], can be written as

$$\frac{\mathcal{J}_{v,1}}{\mathcal{J}_{v,1} + r_m \mathcal{J}_{v,2}} = x_{1,w}. \tag{84}$$

The minimum wall temperature for nucleation onset ($T_{w,n}$) corresponds to the case $\eta_n = 0$ (cf. section 2.7). That is, imposing $ds/d\eta = 0$ at $\eta = 0$ and using the equations of section 4.1, for $T_w = T_{w,n}$, we find:

$$Sc_1 \mathcal{J}_{v,1} = \left. \frac{d\omega_{v,1}^{eq}}{d\eta} \right|_{\eta=0} - \frac{r_m \mathcal{J}_{v,2} \omega_{v,2;w}^{eq}}{\mathcal{J}_{v,1} + r_m \mathcal{J}_{v,2}} \cdot \left. \frac{d}{d\eta} \left(\frac{\omega_{v,1}^{eq}}{\omega_{v,2}^{eq}} \right) \right|_{\eta=0} - \frac{\omega_{v,1;w}^{eq}}{\omega_{v,2;w}^{eq}} Sc_2 \mathcal{J}_{v,2}. \tag{85}$$

Therefore, $T_{w,n}$ corresponds to the case when the deposition values $\mathcal{J}_{v,i}$ given by [66] also satisfy [85]. For $T_w < T_{w,n}$, a two-phase region exists near the wall and corresponding deposition rates should be computed using the equations presented in this section.

In this paper we have provided illustrative results only for the values of the Euler parameter $m = 0$, 1/3 and 1, for which the dimensionless stream function, f, is tabulated (e.g. Schlichting 1979). When the value of f was required at a non-tabulated value of η, we used a Taylor expansion employing the values of f, f', f'' and the corresponding value of f''' from [38] at the closest tabulated value of η. All integrals were calculated using Simpson's algorithm and the local temperature was computed from [42] with $\theta(\eta)$ given by [45].

To obtain the deposition rates, for given T_w and mainstream conditions, the following steps are followed:

1. Given the molecular transport parameters Pr and Sc_i, compute δ_T and $\delta_{v,i}(0)$ as indicated at the end of section 4.1.
2. The dimensionless deposition rates without condensation, are calculated by solving the algebraic system comprised by [66], for $i = 1$, 2, [60] and [61].
3. It can be shown that when condensation within the BL is not possible, l.h.s. < r.h.s. in [85], and the opposite is true when droplets can form. Thus, the values obtained in step 2 can be used in [85] to test the possibility of a two-phase region near the wall.

4. If l.h.s. > r.h.s. in [85] the dimensionless deposition rates with condensation are calculated using the equations given in section 4.2 as follows:
   (a) Choosing a value of η_n, the values of x_1, $dx_1/d\eta$, $d^2x_1/d\eta^2$, $\omega_{c,1}$ and $d\omega_{c,1}/d\eta$ at η_n are calculated from [74], [75], [70], [78] and [71], respectively.
   (b) Equations [70] and [71] are integrated using a fourth-order Runge–Kutta method (as in normally done, the system was transformed to a system of three first-order ODEs by splitting [70] in two ODEs, using the new variable $z = dx_1/d\eta$); starting at the chosen value of η_n until the wall ($\eta = 0$) is reached.
   (c) Once the wall is reached, [84] is checked. If it is not satisfied, a new value of η_n is chosen and steps 4(a)–(c) repeated until [84] is satisfied to the required precision.
   (d) For this value of η_n, the deposition rates [83] are calculated.

5. RESULTS AND DISCUSSION

For illustrative purposes, we present here some numerical results corresponding to *dilute K_2SO_4* (denoted by subscript 1) *and Na_2SO_4* (subscript 2), vapors, with the inert "carrier" gas being air at atmospheric pressure. Estimated values of the thermodynamic and transport properties are given in appendix A. The mainstream temperature is taken as 1700 K and the mass fraction of K_2SO_4 at mainstream is fixed at $\omega_{v,1;\infty} = 4 \times 10^{-2}\omega_{v,1}^{eq}(T_\infty)$. Using the values given in appendix A, this corresponds to $\omega_{v,1;\infty} \approx 1.91 \times 10^{-3}$. We are mainly interested in the variation of deposition rates and BL structure when the amount of the second condensible vapor (Na_2SO_4) in the mainstream is increased. This amount will be indicated by the value of the ratio $p_{v,2;\infty}/p_{v,1;\infty}$ that represents the molar concentration of Na_2SO_4 with respect to the molar concentration of K_2SO_4 at mainstream.

Three different values of the droplet thermophoretic parameter α will be considered: $\alpha = 0.5$ (close to the corresponding theoretical limit for particles in the free-molecular regime); $\alpha = 0.1$ [which appears (Castillo & Rosner 1988a) to provide a good estimate based on experimentally observed deposition rates of Na_2SO_4 condensate particles]; and a lower value of $\alpha = 0.01$ (which might describe the behavior of high thermal conductivity condensate particles in the near-continuum limit).

5.1. Deposition on the Wall

Figures 3–5 depict the deposition rate of K_2SO_4 for a fixed wall temperature, $T_w = 1400$ K and $m = 0$, 1/3 and 1, respectively, as a function of the ratio $p_{v,2;\infty}/p_{v,1;\infty}$. For the lower values of $p_{v,2;\infty}/p_{v,1;\infty}$, condensation within the BL is not possible and the results are obtained as indicated in section 4.1. But beyond a threshold value of $p_{v,2;\infty}/p_{v,1;\infty}$ (indicated by a vertical line in the figures) BL condensation takes place. If even in this case condensation within the BL is not allowed, the deposition rate for this FBL (obtained as described in section 4.1) is given by the dashed line in each figure, showing that $\mathcal{J}_1$ is a continuously increasing function of the molar concentration of the second vapor at mainstream (when the molar concentration of vapor 1 is kept constant). When BL condensation takes place and LTE is attained between the condensed droplets and the surrounding vapor (section 4.2), there are two contributions to the total deposition rate of condensible material, the deposition in vapor form $\mathcal{J}_{v,1}$ represented in the figures by dotted lines, and the deposition in droplets, $\mathcal{J}_{c,1}$. Adding both contributions we get the total deposition rate $\mathcal{J}_1$, depicted by the solid lines for the three values of α considered. For the three vlaues of m considered, it is observed that the qualitative behavior is completely similar. Thus, $\mathcal{J}_{v,1}$ decreases with $p_{v,2;\infty}/p_{v,1;\infty}$ and increases as α decreases (this dependence on α is the opposite for $\mathcal{J}_{v,2}$ and the particular behavior is connected to the change in the deposit composition). On the other hand, the contribution $\mathcal{J}_{c,1}$ decreases as α decreases because the thermophoretic velocity of the droplets diminishes and the droplets are therefore less effective in bringing material to the wall (decreasing the value of $\mathcal{J}_c$). The curves are continuous at the beginning of condensation (except the singular case $\alpha = 0$), where $\mathcal{J}_{c,1} \to 0$. When condensation takes place the diminishing value of $\mathcal{J}_1$ with respect to the FBL value is very important. [For instance, for $m = 1$, $\alpha = 0.1$, $p_{v,2;\infty}/p_{v,1;\infty} = 0.2$, it turns out that $\mathcal{J}_1(\text{LTEBL})/\mathcal{J}_1(\text{FBL}) \approx 0.57$.] For certain values of α and $p_{v,2;\infty}/p_{v,1;\infty}$, the deposition rate, $\mathcal{J}_1$, can lie even below the value for the case when the second vapor is absent ($p_{v,2;\infty} = 0$).

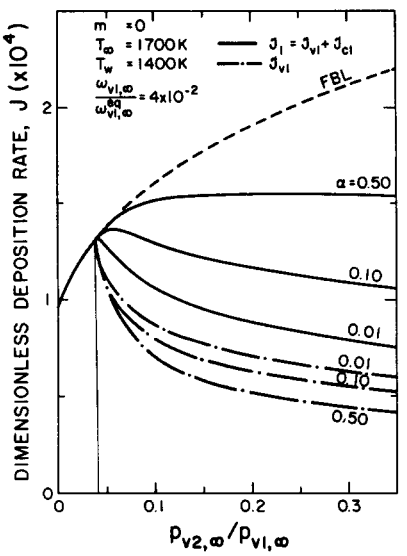

Figure 3. Dependence of the total deposition rate of K_2SO_4, $\mathcal{J}_l$, as a function of the relative mole fraction of Na_2SO_4 in the mainstream, for different values of the condensate thermophoretic parameter α. Conditions: $T_\infty = 1700$ K, $T_w = 1400$ K, $\omega_{v,l;\infty} = 4 \times 10^{-2}\omega^{eq}_{v,l}(T_\infty)$, flat plate collector ($m = 0$).

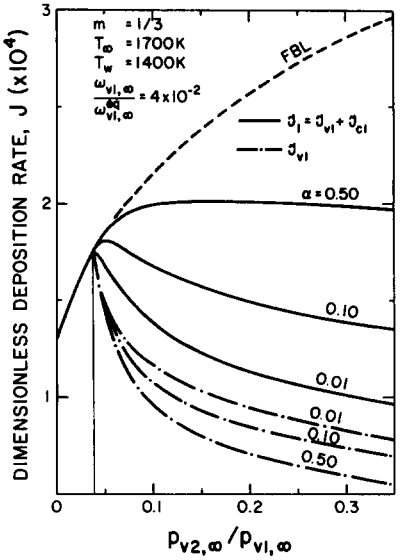

Figure 4. Dependence of the total deposition rate of K_2SO_4, $\mathcal{J}_l$ as a function of the relative mole fraction of Na_2SO_4 in the mainstream, for different values of the condensate thermophoretic parameter α. Conditions: $T_\infty = 1700$ K, $T_w = 1400$ K, $\omega_{v,l;\infty} = 4 \times 10^{-2}\omega^{eq}_{v,l}(T_\infty)$, axisymmetric stagnation point collector ($m = 1/3$).

The relative deposition of the second material, $\mathcal{J}_2/\omega_{v,2;\infty}$ (normalized with respect to $\omega_{v,2;\infty}$ to take into account that $\omega_{v,2;\infty}$ is proportional to $p_{v,2;\infty}$ and therefore is not constant), behaves in a very similar way, and its value, for $m = 1$ and the same conditions as in figure 5, is presented in figure 6. (The value for $p_{v,2;\infty} = 0$ has been obtained by extrapolation.) When condensation within the BL takes place the deposition rate in vapor form $\mathcal{J}_{v,2}$ decreases as α decreases (as opposite to $\mathcal{J}_{v,1}$), only the value for $\alpha = 0.5$ has been represented in the figure because the change with α is very small and the different lines would be indistinguishable with the scale used. The contribution $\mathcal{J}_{c,2}$ also decreases with α decreases. On the other hand, the diminishing value of $\mathcal{J}_2$ with respect

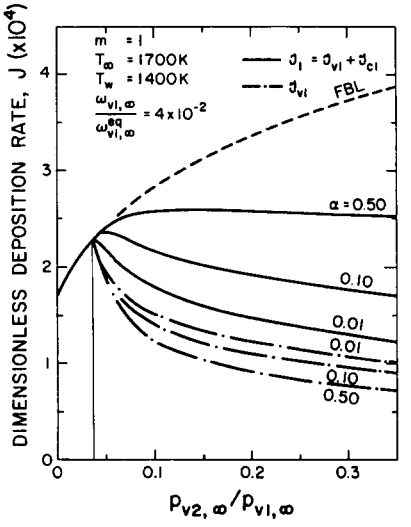

Figure 5. Dependence of the total deposition rate of K_2SO_4, $\mathcal{J}_l$, as a function of the relative mole fraction of Na_2SO_4 in the mainstream, for different values of the condensate thermophoretic parameter α. Conditions: $T_\infty = 1700$ K, $T_w = 1400$ K, $\omega_{v,l;\infty} = 4 \times 10^{-2}\omega^{eq}_{v,l}(T_\infty)$, two-dimensional (planar) stagnation line collector ($m = 1$).

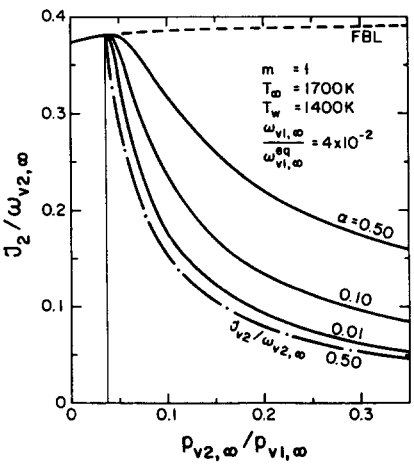

Figure 6. Relative deposition rate of Na_2SO_4, $\mathcal{J}_2/\omega_{v,2;\infty}$, for a constant amount of K_2SO_4 in the mainstream; $\omega_{v,l;\infty} = 4 \times 10^{-2}\omega^{eq}_{v,l}(T_\infty)$, as a function of the relative mole fraction of Na_2SO_4 in the mainstream, for different values of the condensate thermophoretic parameter α. Conditions: $T_\infty = 1700$ K, $T_w = 1400$ K, two-dimensional (planar) stagnation line collector ($m = 1$).

to the FBL value is even more dramatic [for $m = 1$, $\alpha = 0.1$, $p_{v,2;\infty}/p_{v,1;\infty} = 0.2$, it results $\mathscr{J}_2(\text{LTEBL})/\mathscr{J}_2(\text{FBL}) \approx 0.35$], leading to a deposit richer in K_2SO_4 in LTEBL with respect to the FBL case [for the conditions indicated above: $x_{1,\text{dep}}(\text{FBL}) = 0.693$ and $x_{1,\text{dep}}(\text{LTEBL}) = 0.788$].

In figure 7, the deposition rate of K_2SO_4 is presented for $m = 1$ and $\alpha = 0.1$, and different wall temperatures, T_w. The dashed lines depict FBL values and the solid lines correspond to LTEBL. The dotted line represents the locus of BL condensation onset. It is interesting to note that this line does *not* correspond to the line of maximum deposition rate for each surface temperature. The behavior is similar to that presented in figure 5. The influence of condensation upon $\mathscr{J}_1$ is seen to be more important for the lower wall temperatures.

The values of η_n corresponding to figure 7 are plotted in figure 8. At the beginning of condensation (dotted line in figure 7), $\eta_n = 0$. With further increases in the amount of the second condensible material in the mainstream, or decreases in the wall temperature, T_w, the "interface" between the single-phase region and the two-phase region (section 4.2) detaches from the wall and moves away from it, expanding the two-phase region (section 2.7).

5.2. *Boundary Layer Structure*

As a consequence of the condensation phenomena within the BL, the spatial distribution of condensible material changes. As an example, in figure 9 the vapor mass fraction profiles are presented for the conditions specified in figure 5 [i.e. $m = 1$, $T_\infty = 1700$ K, $T_w = 1400$ K, $\omega_{v,1;\infty} = 4 \times 10^{-2}\omega^{eq}_{v,1}\{T_\infty\}$] and $p_{v,2;\infty} = 0.2p_{v,1;\infty}$, $\alpha = 0.1$. Again, the dashed lines correspond to FBL and solid lines to LTEBL. Of course, in any case both $\omega_{v,1}$ and $\omega_{v,2}$ tend to their mainstream values for large values of η ($\omega_{v,1;\infty} = 1.913 \times 10^{-3}$ and $\omega_{v,2;\infty} = 3.119 \times 10^{-4}$, respectively). The interface between the single-phase ($\eta > \eta_n$) and the two-phase ($\eta < \eta_n$) region is located at $\eta_n \approx 0.933$. The profile of $\omega_{v,1}$ changes slightly, being appreciably different to this scale, only in the vicinity of the wall. The influence on $\omega_{v,2}$ is even more appreciable, extending well beyond the position at which condensation begins ($\eta = \eta_n$). It is observed that at the wall the slopes of $\omega_{v,1}$ and $\omega_{v,2}$ are smaller for an LTEBL than for an FBL, leading to a smaller deposition rate (in vapor form) for an LTEBL and also, at the wall, $\omega_{v,1}(\text{LTEBL}) > \omega_{v,1}(\text{FBL})$ and therefore, as required by the boundary condition [61], (that both LTEBL and FBL must verify), $\omega_{v,2}(\text{LTEBL}) < \omega_{v,2}(\text{FBL})$, indicating that the deposit, in LTEBL, is relatively richer in component 1 (K_2SO_4).

Finally, the distributions of condensible materials (for LTEBL) in vapor and condensed form inside the two-phase region ($\eta < \eta_n$), are plotted in figure 10 for the same conditions corresponding

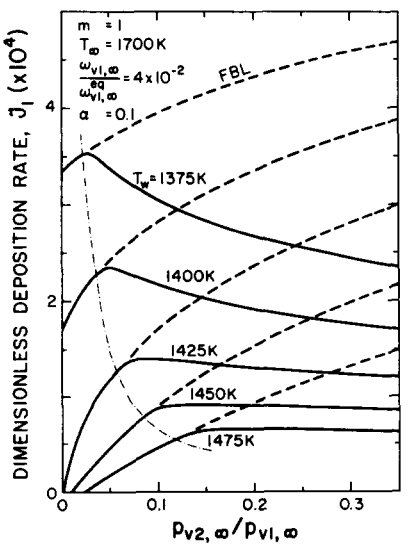

Figure 7. Total deposition rate of K_2SO_4, $\mathscr{J}_1$, as a function of the relative molar fraction of Na_2SO_4 in the mainstream, for various wall temperatures. Conditions: $T_\infty = 1700$ K, $\omega_{v,1;\infty} = 4 \times 10^{-2}\omega^{eq}_{v,1}\{T_\infty\}$, $\alpha = 0.1$, two-dimensional (planar) stagnation line collector ($m = 1$).

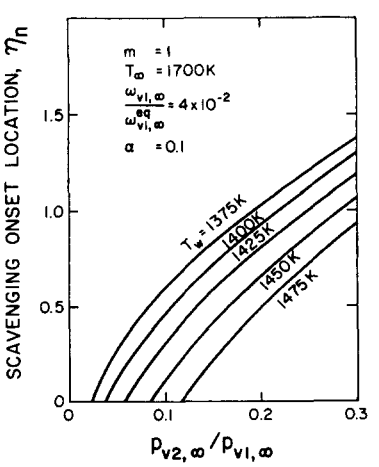

Figure 8. Position of the "interface" between the single phase region ($\eta > \eta_n$) and the two-phase region ($\eta < \eta_n$) for the conditions specified in figure 7.

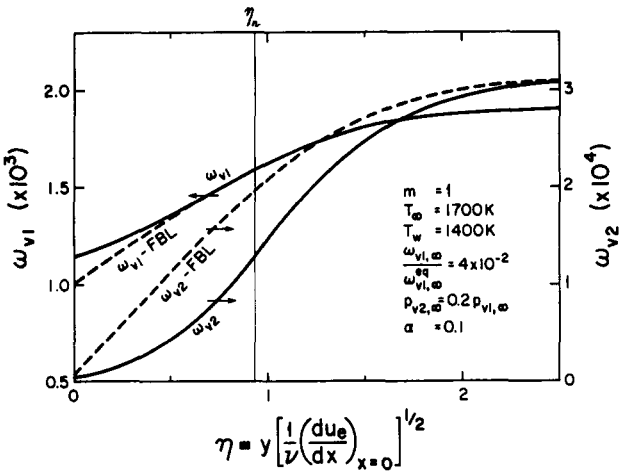

Figure 9. Vapor mass fraction profiles within the BL for the FBL and LTEBL limiting cases. Conditions: $T_\infty = 1700$ K, $T_w = 1400$ K, $\omega_{v,1;\infty} = 4 \times 10^{-2}\omega^{eq}_{v,1}\{T_\infty\}$, $p_{v,2;\infty} = 0.2p_{v,1;\infty}$, $\alpha = 0.1$, two-dimensional (planar) stagnation line collector ($m = 1$).

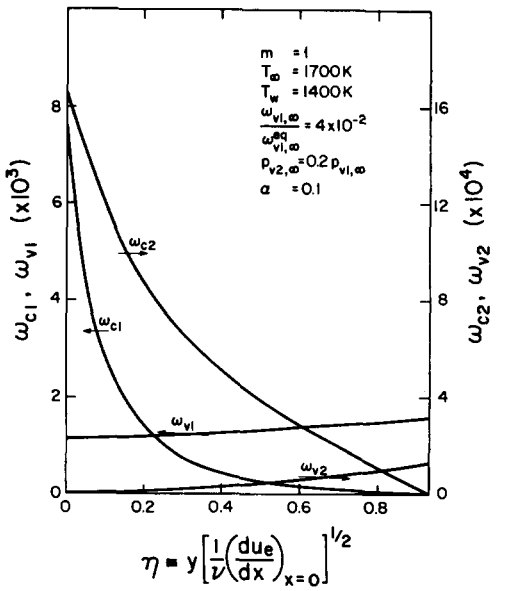

Figure 10. Distribution of condensible material ($K_2SO_4 = 1$, $Na_2SO_4 = 2$) within the two-phase region ($\eta < \eta_n$) in vapor form ($\omega_{v,i}$) and in condensate form ($\omega_{c,i}$). Conditions: $T_\infty = 1700$ K, $T_w = 1400$ K, $\omega_{v,1;\infty} = 4 \times 10^{-2}\omega^{eq}_{v,1}\{T_\infty\}$, $p_{v,2;\infty} = 0.2p_{v,1;\infty}$, $\alpha = 0.1$, two-dimensional (planar) stagnation line collector ($m = 1$).

to figure 5. Both $\omega_{c,1}$ and $\omega_{c,2}$ start from a zero value at $\eta = \eta_n$ (they are equal to zero for $\eta > \eta_n$, and their slopes are discontinuous at $\eta = \eta_n$), and continuously increase up to the wall ($\eta = 0$). In the very vicinity of the wall the amount of condensible materials in droplet form is much larger than in vapor form. The droplets, driven by thermophoresis, move toward the wall slower than the vapor does by Fick diffusion. As a consequence, droplets are not so effective in bringing condensible material to the wall, therefore reducing the total deposition rate of both condensible materials (with respect to the FBL case in which droplets do not exist and the transport mechanism to the wall is exclusively Fick diffusion), as was observed in figures 5 and 6.

6. CONCLUSIONS—IMPLICATIONS

Until now, multicomponent vapor deposition rates under conditions in which the mixture "dew point" is achieved *within* the thermal BL, could not be predicted, primarily because of the difficulty of predicting the contribution associated with the collection of the newly formed solution condensate aerosol. Here we provide a rational yet tractable method for making such predictions in the limiting case that vapor/liquid equilibrium is maintained in the two-phase (inner) region of the LBL, and the dispersed solution condensate is collected by *thermophoresis*. Illustrative calculations are included for the deposition of sodium sulfate and potassium sulfate from initially undersaturated streams of combustion products exposed to actively cooled solid targets representing turbine blades (above the *binary* $Na_2SO_4 + K_2SO_4$ melting point). This system has also been studied experimentally in this laboratory (Liang *et al.* 1988)—indeed these experiments motivated and can be understood and extrapolated with the help of the present theoretical developments.

In the present work we have numerically considered only dilute binary vapor systems under conditions such that the mainstream is undersaturated, and equilibrium occurs in the thermal BL to form ideal solution droplets. In applying this formalism to systems of current practical importance we anticipate that it will be necessary to correct further for the facts that: (a) real alkali vapor systems are partially dissociated and interact chemically with species [e.g. $H_2O(g)$] normally present in the combustion products; and (b) real alkali sulfate solutions are slightly non-ideal, thermodynamically. Simple methods for making these necessary "corrections" have recently been developed and are presented elsewhere (e.g. Roy *et al.* 1988; Liang *et al.* 1988).

This deposition rate analysis and its predecessor for undersaturated unary vapor mainstreams (Castillo & Rosner 1988a) provide the theoretical background necessary to examine the consequences of relaxing the simplifying assumption that the dispersed condensate surface area per unit volume is large enough to maintain vapor/condensate equilibrium everywhere within the thermal BL (Castillo & Rosner 1988b). While non-equilibrium situations will undoubtedly be encountered in specific applications, we believe that the simplicity and generality of the present asymptotic cases, and the insights obtained from their investigation, amply justify their quantitiative examination here.

With the help of the abovementioned studies a comprehensive, quantitative picture of the important regimes of multicomponent vapor and/or particle deposition is beginning to emerge, including their interesting mutual interactions within BLs. Since these convective mass transfer phenomena appear in so many technologies, this understanding should ultimately pay handsome dividends in the form of improved deposition rate predictability and control.

Acknowledgements—We gratefully acknowledge many helpful discussions with our colleagues J. Fernandez de la Mora (ME Dept, Yale University), B. Liang (University of California—Berkeley), R. Nagarajan (IBM, San Jose), H. M. Park (Brown University) and S. A. Gökoğlu (NASA-Lewis Research Lab.). We are also indebted to the U.S. Government agencies (NASA, DOE-METC and DOE-PETC) whose financial support made possible these fundamental studies and their publication.

This work was supported, in part, by DOE-METC (Contract DE-AC21-85MC22075) and NASA-Lewis Research Center (Grants NAG-3-590 and NAG-3-884).

NOMENCLATURE

a = Constant in [31]
A = Function defined by [50]
b = Constant in [67]
B = Function defined by [51]
D = Fick diffusion coefficient
f = Blasius non-dimensional stream function
$\mathbf{j}''$ = Diffusion mass flux vector
$\mathcal{J}$ = Non-dimensional mass flux at the wall; see [57]
m = Euler parameter defined in [31], $m = \beta/(2-\beta)$
$M_{v,i}$ = Molecular weight of vapor i
N = Number of condensible vapor species
$\mathbf{n}$ = Unit normal vector
n_i = Moles of vapor i
p = Total pressure
$p_{v,i}$ = Vapor pressure of component i
Pr = Prandtl number ν/α_h of gas mixture
$\dot{r}_i'''$ = Local mass consumption rate of vapor i (per unit volume)
r_m = Molecular mass ratio, $M_{v,1}/M_{v,2}$
R = Universal gas constant
s = Saturation ratio; [5]
Sc_i = Schmidt number for vapor i; $\nu/D_{v,i}$
t = Time
T = Local temperature
u_e = External (potential) flow velocity along x
$\mathbf{v}$ = Velocity vector (x-component u and y-component v)
x = Distance along the wall measured from the forward stagnation point; figure 2
x_i = Molar fraction of component i in the liquid phase
y = Distance normal to the wall; figure 2

Greek symbols

α = Normalized thermophoretic coefficient; $\alpha_T D_{drop}/\nu$
α_h = Thermal diffusivity of gas mixture

α_T = Thermophoretic factor (dimensionless)
β = Included angle of wedge (as multiple of π); figure 2
Γ = Normalized vapor mass fraction; [64]
δ_T = Parameter defined by [46]
δ_i = Function defined by [65]
η = Similarity variable; [34]
η_∞ = Value of η defined by [67]
θ = Dimensionless temperature; [45]
ν = Momentum diffusivity (kinematic viscosity) of the gas mixture
ρ = Density of mixture
ψ = Stream function; [35]
$\omega_{v,i}$ = Mass fraction of vapor i; $\rho_{v,i}/\rho_G$
$\omega_{c,i}$ = Mass fraction of condensate component ; $\rho_{c,i}/\rho_G$
$\dot{\omega}_i'''$ = Dimensionless vapor consumption rate; [48]
ξ, ϕ, φ = Dummy (integration) variables

Subscripts

e = At outer edge of the momentum BL
c = Condensate phase (droplets)
dep = Liquid deposit
diff = Diffusion
drop = Droplet
G = Total gas mixture (carrier gas + vapor)
inert = Inert (carrier) gas
i, j = Condesible component i, j
n = At the "interface" between the two-phase (2ϕ) and the single-phase (1ϕ) regions
T = Thermophoretic
v = Vapor
w = At the wall ($y = 0$)
∞ = At the mainstream ($y \to \infty$)

Superscripts

eq = Equilibrium value over pure liquid i
$2\phi, 1\phi$ = Refers to a quantity on the "interface" between the two-phase and the single-phase region
$'$ = Derivative with respect to η

Abbreviations

BC = Boundary condition
BL = Boundary layer
FBL = Frozen (source-free) boundary layer
l.h.s. = Left-hand side
LTE = Local thermodynamic equilibrium
ODE = Ordinary differential equation
PDE = Partial differential equation
r.h.s. = Right-hand side

REFERENCES

CASTILLO, J. L. & ROSNER, D. E. 1988a Theory of surface deposition from a unary dilute vapor-containing stream, allowing for condensation within the laminar boundary layer. *Chem. Engng Sci.* In press.

CASTILLO, J. L. & ROSNER, D. E. 1988b A nonequilibrium theory of surface deposition from particle-laden, dilute condensible vapor-containing laminar boundary layers. *Int. J. Multiphase Flow* **14**, 99–120.

CUTLER, A. J. B. 1983 Molten sulfates. In *Molten Salt Techniques*, pp. 111–135. Pergamon Press, New York.

EVANS, H. L. 1961 Mass transfer through laminar boundary layers—3a. Similar solution of the b-equation when $B = 0$ and $\sigma > 0.5$. *Int. J. Heat Mass Transfer* **3**, 26–41.

FERNANDEZ DE LA MORA, J. & ROSNER, D. E. 1982 Effects of inertia on the diffusional deposition of small particles to spheres and cylinders at low Reynolds numbers. *J. Fluid Mech.* **125**, 379–396.

FUCHS, N. A. 1964 *The Mechanics of Aerosols*. Pergamon Press, New York.

GÖKOĞLU, S. A. & ROSNER, D. E. 1984 Engineering correlations of variable-property effects on laminar forced convection mass transfer for dilute vapor species and small particles in air. Report NASA CR-168322.

KOHL, F. J., STEARNS, C. A. & FRYBURG, G. C. 1975 Sodium sulfate: vaporization thermodynamics and role in corrosion flames. In *Metal–Slag–Gas Reactions and Processes* (Edited by FOROULIS, Z. A. & SMELTZER, W. W.), pp. 649–664. The Electrochemical Society, Princeton, N.J.

LIANG, B. L. & ROSNER, D. E. 1987 Laboratory studies of binary salt CVD in combustion gases environments. *A.I.Ch.E. Jl* **33**, 1937–1948.

LIANG, B. L., GOMEZ, A., CASTILLO, J. L. & ROSNER, D. E. 1988 Experimental studies of nucleation phenomena within thermal boundary layers—influence on chemical vapor deposition rate processes. *Proc. A. Mtg of the American Society of Aerosol Research*, Paper A5A. *Chem. Engng Commun.* In press.

PRAUSNITZ, J. M., ECKERT, C. A. ORYE, R. V. & O'CONNELL, J. P. 1967 *Computer Calculations for Multicomponent Vapor–Liquid Equilibria*. Prentice-Hall, Englewood Cliffs, N.J.

ROSNER, D. E., 1986 *Transport Processes in Chemically Reacting Flow Systems*. Butterworths, Stoneham, Mass. (reprinted 1988).

ROSNER, D. E. 1988 Experimental and theoretical research on the deposition dynamics of inorganic compounds from combustion gases. *PhysicoChem. Hydrodynam.* **10.** In press.

ROSNER, D. E., CHEN, B. K., FRYBURG, G. C. & KOHL, F. J. 1979 Chemically frozen multicomponent boundary layer theory of salt and/or ash deposition rates from combustion gases. *Combust. Sci. Technol.* **20**, 87–106.

ROSNER, D. E., GÜNES, D. & ANOUS, N. 1983 Aerodynamically-driven condensate layer thickness distributions on isothermal cylindrical surfaces. *Chem. Engng Commun.* **24**, 275–287.

ROY, R., LIANG, B. L. & ROSNER, D. E. 1988 Simplified dew point predictions for N-trace salt-containing non-ideal condensates in high temperature reactive vapor environments. *Chem. Engng Commun.* In press.

SCHLICHTING, H. 1968 *Boundary Layer Theory*, 6th ed. McGraw-Hill, New York. (See also 7th edn, 1979.)

SMITH, J. M. & VAN NESS, H. C. 1975 *Introduction to Chemical Engineering Thermodynamics*, 3rd edn, Chaps 7 and 8. McGraw-Hill, New York.

SPALDING, D. B. & EVANS H. L. 1961 Mass transfer through laminar boundary layers—3. Similar solutions of the b-equation. *Int. J. Heat Mass Transfer* **2**, 314–341.

STUDZINSKI, W., ZAHORANSKY, R. A., WITTING, S. L. K. & BARSCHDORFF, D. 1984 Droplet formation and growth in condensing binary vapors. *Int. J. Heat Mass Transfer* **27**, 451–461.

TALBOT, L. 1981 Thermophoresis—a review. In *Rarefied Gas Dynamics*, Part I (Edited by FISHER, S. S.). *Prog. Astronaut. Aeronaut.* **74**, 467–488.

APPENDIX A

Input Data—Illustrative Case

All figures presented in this paper correspond to dilute K_2SO_4 (denoted by subscript 1) and Na_2SO_4 (subscript 2) vapors, with the inert "carrier" gas being air at atmospheric pressure. According to assumption A.5 the gas thermodynamic properties are considered constant and equal to their values at the mainstream temperature, T_∞. Thus, we take

$$\rho = \frac{0.353}{T_\infty} \qquad [\text{g/cm}^3].$$

The temperature dependence for each $p_{v,i}^{eq}$ is taken to be of the Clausius–Clapeyron form:

$$p_{v,i}^{eq}(T) = \exp\left(\gamma_i - \frac{\Lambda_i}{RT}\right) \quad [\text{dyn/cm}^2].$$

These equations were used in the calculation of $\omega_{v,i}^{eq}(T)$, [3], with the values

$$M_{v,1} = 174.26 \text{ g/mol} \quad \text{and} \quad M_{v,2} = 142.05 \text{ g/mol}.$$

From Cutler (1983),

$$\gamma_1 = 26.2 \quad \text{and} \quad \Lambda_1/R = 2.925 \times 10^4 \text{K};$$

and from Kohl *et al.* (1975),

$$\gamma_2 = 25.05 \quad \text{and} \quad \Lambda_2/R = 3.325 \times 10^4 \text{K}.$$

While these values are assumed in the illustrative calculations of this paper it should be recognized that because of dissociation and chemical reactions (e.g. with water vapor) the effective values of γ and (to a lesser extent) Λ/R will depend somewhat on combustion conditions (e.g. Kohl *et al.* 1975; Roy *et al.* 1988). The Prandtl number was taken equal to 0.7 (air) and the vapor Schmidt numbers, $Sc_1 = 2$ and $Sc_2 = 1.8$. For these values of Pr and Sc_i the following values of δ_T, [46], and $\delta_i(0)$, [65], were obtained for the values of the Euler parameter m of principal interest here:

	δ_T (Pr = 0.7)	$\delta_1(0)$ (Sc = 2)	$\delta_2(0)$ (Sc = 1.8)
$m = 0$ (flat plate)	3.41669	2.36793	2.45525
$m = 1/3$ (axisymm. stag. pt)	2.60279	1.75597	1.82522
$m = 1$ (planar stag. pt)	2.01669	1.34459	1.39912

APPENDIX B

Solution by Quadratures

When a two-phase region exists in the vicinity of the wall, the solution of [47] and [49], for $\eta \leqslant \eta_n$, can be written in the form

$$\omega_{v,i} = \int_\eta^{\eta_n} d\beta \int_\beta^{\eta_n} Sc_i \dot{\omega}_i'''(\varphi) \exp\left[\frac{m+1}{2} Sc_i \cdot \int_\beta^\varphi f(\xi)\, d\xi\right] d\varphi - \left.\frac{d\omega_{v,i}}{d\eta}\right|_{\eta_n} \int_\eta^{\eta_n} \exp\left[\frac{m+1}{2} Sc_i \cdot \int_\varphi^{\eta_n} f(\xi)\, d\xi\right] d\varphi + \omega_{v,i,n} \quad [B.1]$$

and

$$\omega_{c,i} = \int_\eta^{\eta_n} \frac{\dot{\omega}_i'''(\varphi)}{A(\varphi)} \cdot \exp\left[\int_\eta^\varphi \frac{B(\xi)}{A(\xi)} \cdot d\xi\right] d\varphi \quad [B.2]$$

with $\dot{\omega}_i'''(\eta)$ such that the local equilibrium conditions given by [53] and [54] are fulfilled everywhere within the two-phase region.

We attempted to carry out these integrals numerically using a Simpson algorithm (except for the integrals in which the source term $\dot{\omega}_i'''$ appears, where a simple trapezoidal rule was used and [53] and [54] were imposed on the value of $\dot{\omega}_i'''$ at the end of each integral step). The solution was found to be numerically unstable, with oscillations appearing in the values of the different variables within the two-phase region. For this reason, the direct Runge–Kutta integration method presented in section 4.2 was used instead, yielding a perfectly stable solution.

APPENDIX C

Role of Nucleation Kinetics Restrictions

It is true that for systems free of condensation nuclei, vapor condensation does not take place precisely when the value $s = 1$ is reached, due to the activation barrier associated with the surface

free energy of embryonic droplets. The *kinetics* of homogeneous nucleation in condensing binary vapors has been recently analyzed by Studzinski *et al.* (1984), who present the nucleation rate equation (rate of generation of "critical" nuclei) as well as the rate equations governing droplet size, composition and temperature. However, when active foreign bodies *are* present, these provide favorable sites for vapor molecules to initiate the new phase. If the number density of foreign condensation nuclei is adequate, the vapor condensation will occur in such a way that the value $s = 1$ is approximately maintained. This kind of nucleation is properly called *heterogeneous* nucleation. Except for scrupulously arranged laboratory experiments, heterogeneous nucleation is indeed most often observed. The contamination level associated with most combustors is expected to allow our assumption A.4 of condensation at local equilibrium to be a useful first approximation.

Recently, Castillo & Rosner (1988b) have presented an analysis in which assumption A.4 has been relaxed for a *unary* dilute vapor. Accordingly, that analysis can be used to define the range of validity of the present approximation in terms of the concentration and size of the mainstream particles which will serve as condensation nuclei.